Electromigration-driven weak resistance switching in high-temperature superconducting devices

Stefan Marinković,[1,*] Daniel Stoffels,[1,†] Simon Collienne,[1] Alejandro Fernández-Rodríguez,[2] Narcís Mestres,[2] Anna Palau,[2,‡] and Alejandro V. Silhanek[1,§]

[1] *Experimental Physics of Nanostructured Materials, Department of Physics, Université de Liège, B-4000 Sart Tilman, Belgium*

[2] *Institut de Ciència de Materials de Barcelona, ICMAB-CSIC, Campus UAB, 08193 Bellaterra, Spain*

(Dated: October 10, 2024)

Complex oxides are at the heart of modern functional material developments. In particular, the perovskite ABO_3 structure is seen in compounds used in oxide solar cells, resistive memories, fuel cell catalysts, superconducting tapes, quantum bits and programmable magnets, making it one of the most studied material families. One important advantage of these systems is that their properties may be controlled *in situ* to change between various electronic states, usually by means of thermal or electric conditioning. In this work, we investigate the two-terminal resistive switching properties of the perovskite-like oxide $YBa_2Cu_3O_{7-\delta}$ when the system is driven by electric current. We perform all-electrical switching to characterize and control low-amplitude resistance changes, and we implement finite element modelling to explain how these effects can be properly accounted for by oxygen-vacancy counterflow induced by electric bias. The presented research sheds new light on the bulk displacement of oxygen atoms in perovskite materials with potential for sensing and memory technologies.

I. INTRODUCTION

Complex oxides represent a family of materials offering a rich and diverse cast of physical phenomena with potential to be exploited in electronic and energy applications, ranging from superconductivity, ferroelectricity to giant magnetoresistance.[1] In particular, the structural subfamily ABO_3 known as perovskites, has provided numerous promising candidates for photovoltaics, sensors, catalysts and memories. By and large, such materials have complex phase diagrams exhibiting a plethora of functional phases that can be accessed by changing temperature, pressure, strain, electric field, composition, or doping [2].

Some of these oxides form non-stoichiometric crystals, meaning that their structure may exist in a single condensed phase across a range of compositions, most commonly of the oxygen atom.[3] In such cases, charge neutrality is maintained through the distribution of oxygen vacancies in the crystal. This is the case of the oxide $YBa_2Cu_3O_{7-\delta}$ (YBCO), which exhibits superconducting behavior as long as the value of δ lies below ~ 0.45, with the superconducting critical temperature T_c increasing (and normal state resistivity ρ decreasing) as δ falls.[4]

It naturally follows that gaining mastery over the oxygen distribution (commonly referred to as *doping*) in such materials would allow one to control all other functionalities the material might hold. Although it is possible to synthesize YBCO samples with varying doping levels, there is substantial interest in the concept of manipulating the oxygen content in situ using electric actuation. Studies have employed voltage gates with ferroelectric [5], or dielectric layers, such as ionic liquids [6, 7], to locally manipulate the δ. Voltage-induced electrochemical doping has also been observed in YBCO samples using a metallic gate, allowing for manipulation of the oxygen distribution in a volume below the gate [8], which appears to be an appealing mechanism for the design of transistor-like devices [9, 10]. Our approach, in contrast, specifically involves applying current to modulate oxygen doping, potentially engaging different operating mechanisms. Current-driven oxygen migration [11, 12] seems to modulate the oxygen distribution profile in a larger volume and in a more persistent way. This restructuring may still be reversed by inverting the electric current polarity, yet does not relax to the same state as voltage-induced approaches.

The end goal in the research line of current-stimulated oxygen doping is twofold. Firstly, wide composition ranges can be studied in single samples, easing the burden of synthesis and characterization of the material being studied. Secondly, these methodologies show promise in resistive memory applications, as oxides are excellent candidates for non-volatile multi-state memories and integrators. The latter technology specifically exploits the variable resistivity of the material as oxygen is transported in or out of a targeted region in the device.[13]

The study at hand aims to investigate low-amplitude resistance switching in YBCO. Most importantly, the method only relies on electrical current flowing directly through the material to modulate the oxygen doping, all via the phenomenon of selective electromigration. We explore the possibility of inducing a small resistance increase (~ 1 %) followed by a recovery to the initial resistance by applying a bipolar bias current of constant

* smarinkovic@uliege.be; Contributed equally.
† Contributed equally
‡ palau@icmab.es
§ asilhanek@uliege.be

amplitude. We unambiguously demonstrate that the resistance changes are associated with back-and-forth oxygen displacement over long distances ($\sim$ 5 μm) driven by a current-stimulated diffusive mechanism. This is a reminiscent of long-range changes occurring under voltage gating [14, 15]. The slow switching process ($\sim 1-20$ s) can be repeated 10^4 times with high fidelity and little variation of the overall resistance of the device. This fact seems to point to a negligible oxygen loss from the device. Low-temperature measurements show that the procedure also works at 100 K but requires higher drives. The induced small resistance changes have no impact on the superconducting transition. The periodic albeit non-monotonous pattern displayed by the time evolution of the resistance can be properly captured by finite element modeling taking into consideration the interplay between oxygen diffusion, heat equation, a resistivity which depends on the oxygen content, and the specific sample geometry.

II. EXPERIMENTAL

A. Samples

Samples consist of 50-nm-thick films of *c*-axis oriented YBCO, epitaxially grown on $LaAl_2O_3$ (LAO) substrates and patterned into a triple-constriction design shown in Fig. 1. The samples were grown by pulsed laser deposition and exhibited sharp superconducting transitions at 90 K (corresponding to δ=0.05). The inner constriction (green) is 1×5 μm, and the outer ones (left-red and right-blue) are 3×5 μm. The samples were subjected to high current densities (up to 14 MAcm^{-2}) corresponding to colossal power densities ($P \sim 5$ GW/cm^3).

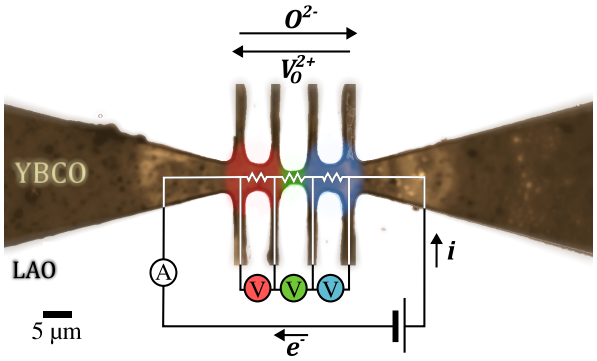

FIG. 1. Sample layout in the form of a triple-constriction where each of the three bridge resistances can be accessed using two of the perpendicular terminals. The colour code associated with the three bridges will be respected throughout the manuscript. The battery indicates what is defined as a positive voltage configuration.

B. Resistive Switching Protocol

Performing reversible switching in oxide systems requires an understanding of operational parameters, principally the required current of electromigration. For this purpose, we determine the onset current for electromigration ($I_{\rm EM}$) by stressing a device with a series of current pulses ($t_{\rm pulse} = 1$ s) of linearly increasing amplitude, as previously described in Ref. [12, 16]. By measuring the resistance of all three constrictions with low current density between the individual pulses, it is possible to separate oxygen diffusion effects from Joule heating and define $I_{\rm EM}$ as the current at which the resistance between pulses of the central bridge R_C has increased by 1 %.

Here, positive current bias, defined by the polarity indicated in Fig. 1, leads to oxygen vacancy displacement from right to left, which manifests itself as a detectable increase of resistance in the central (green) constriction. Simultaneously we observe a resistance increase on the left (red) bridge and a drop of resistance on the right (blue) bridge due to oxygen/vacancy counterflow.[17] Upon reversal of the current polarity, some degree of reversibility has been reported.[17] Motivated by this fact, we explore the cyclic stability and amplitude of the current-driven oxygen selective diffusion by biasing the sample with a square-wave current excitation of alternating polarity.

C. Finite Element Modelling

We resort to finite element modelling to investigate the oxygen concentration and temperature profile of our sample during the experiment, building on a model previously validated in both YBCO[17] and LSMO.[12] We employ the proprietary software suite COMSOL to model the YBCO structure as a continuous two-dimensional isotropic material whose oxygen concentration may vary between $c_{min} = 3.41 \times 10^{28}$ and $c_{max} = 4.01 \times 10^{28}$ ions m^{-3}.[4] These extreme values of c represent YBCO being fully tetragonal ($\delta = 1$, insulating) or orthorhombic ($\delta = 0$, superconducting). We introduce a more convenient derived parameter $x = (c - c_{min})/(c_{max} - c_{min})$ representing the doping, as we consider oxygen to vary only between these two values.[9] In other words, $0 < x < 1$, with $x \to 0$ for an oxygen depleted region and $x \to 1$ for an oxygen rich zone. The temporal evolution of x depends on the electric field as well as on the temperature [17] as described by Eq. 1,

$$\frac{\partial x}{\partial t} = \nabla.(D\nabla x + zuFx\nabla V), \qquad (1)$$

where D is the temperature-dependent diffusion constant governed by the Arrhenius expression $D = D_0 \exp\{(-E_a/k_BT)\}$ with $D_0 = 1.4 \times 10^{-8}$ m^{2}s^{-1}.[18] We consider E_a the activation energy (in eV) and k_B the Boltzmann constant, while $z = -2$ is the charge

number of the oxygen ions, u the Nernst-Einstein ratio ($u = D/RT$) and F the Faraday number. The sign of the effective charge number z determines whether the modelled particles interact with electrons or holes.

The first term on the right-hand side of Eq. 1 describes thermally activated diffusion along concentration gradients, whereas the second one addresses diffusion due to potential gradients (i.e. electric field) and carrier momentum transfer.[19] In addition, the heat transport equation is solved, including Joule effect due to the high current density, implementing an x-dependent resistivity and considering heat evacuation through the substrate. This allows us to obtain the temperature distribution in the system. Then, the Poisson equation is solved to determine the electric potential distribution in the sample alongside the diffusion of oxygen according to Eq. 1. Details on thermal coefficients for substrate and material adapted to YBCO are available in Ref. [17]. The numerical resolution of the coupled system of equations with interdependent parameters is implemented as an iterative segregated solver in COMSOL,[20] streamlining the implementation compared to that presented in Ref. [17] for use against a bipolar square-wave current bias of longer duration. We set the parameters ($E_a = 0.58$ eV, starting oxygenation $x_0 = 0.9$) as to approximate the behavior of our films. The law relating the oxygen content to the YBCO resistivity ρ is described by linearizing the findings given in Ref. [21] for values of $x \in [0.5, 0.9]$. This linear approximation is justified by the fact the exact nature of the $\rho(x)$ functionality seems not to play a significant role in qualitatively reproducing complex switching behaviour.[15] Note that we have considered an isotropic material justified by regular exchange of crystallographic a and b axes. An anisotropic model adapted for untwinned YBCO films has been presented in Ref. [22].

III. RESULTS AND DISCUSSION

A. Experimental results

In order to investigate the degree of control, reversibility, retention, and endurance of the resistive switching caused by selective current-induced oxygen vacancy (V_O^{2+}) electromigration, the following protocol was implemented: First, a constant amplitude current of $I_{\text{app}} = +5.8$ mA is applied across the constrictions while the resistances of each individual bridge are monitored simultaneously. After an initial training phase dominated by thermalisation (see Appendix A), we set a predefined base resistance R_0 as 1% above the low-current resistance of the central bridge. After that, the central resistance R_C starts exhibiting a dome-shape evolution (see green background panels in Fig. 2). The current polarity is reversed upon reaching R_0 on the falling slope of the dome-shaped curve of R_C.

The zooms on the middle column of Fig. 2 show the resistive response of the three bridges for one period of the square-wave excitation (highlighted with a darker background in Fig. 2(a-d)). The observed response is a direct manifestation of an oxygen-vacancy counterflow swaying from left to right and vice-versa. In the positive half-period ($I_{\text{app}} = +5.8$ mA), the dome-shaped curves of the resistance in the central junction (Fig. 2(b)) reveal a deoxygenation front passing through it. The left bridge exhibits a nearly linear increase of resistance as this region becomes progressively populated with oxygen vacancies (Fig. 2(a)). Concomitantly, oxygen atoms migrate towards the symmetrically opposite bridge on the right, which naturally explains its decrease in resistance (Fig. 2(c)). Upon inverting the current polarity (Fig. 2(d)) on the second half-period ($I_{\text{app}} = -5.8$ mA), the outer bridges reverse roles, and the central bridge exhibits a new dome as the deoxygenated phase expands in the opposite direction. Note, however, that the resistance dome on the central bridge reaches a different local maximum amplitude $R_{\max}$ depending on the current polarity and that the R_C domes have a generally slanted shape with the rising side being steeper (positive skewness). This periodic resistance cycling can be repeated without any observed structural damage for a large number of cycles. The maximum number of switching iterations we have tested is $\sim 10^4$.

It is worth noting that the amplitude of the resistance oscillations in the left and right bridges are unequal, even though the number of vacancies/atoms swaying from one side to the other remains the same. This difference reflects an asymmetry in the affected volume between the respective left and right voltage contacts which could arise from uncontrollable inaccuracies in the patterning process or simply be imposed by the initial current polarity.

We should stress the fact that the criterion implemented for switching current polarity is not a fixed period but rather the condition that R_C returns to R_0. In other words, neither the period of the square wave nor the amplitude of the resistance modulations are controlled parameters. This is better illustrated by tracking the evolution of the half-period δt as a function of the switching number, as is shown in Fig. 2(e). Note that δt exhibits an initial sharp decrease before reaching a stable value. We speculate that this behaviour may be caused by the oxygen redistribution which, once established, facilitates faster development of O-V_O^{2+} counterflow during subsequent cycling, somewhat similar to the forming phase in filamentary memristive devices.[23] Eventually, after several thousand switches, irreversible modifications seem to clog the diffusion channels and δt tends to slowly rise.

Figure 2(f,g) show the evolution of respectively δt and $R_{\max}$ as a function of switch number for several current amplitudes. These measurements were sequentially performed on a single sample. For the highest current amplitude (7.25 mA) a rise in δt occurs after ~ 25 switches, whereas for lower currents the initial decrease in δt and $R_{\max}$ are much more pronounced and a subsequent rise is expected to occur later (i.e. at higher switch num-

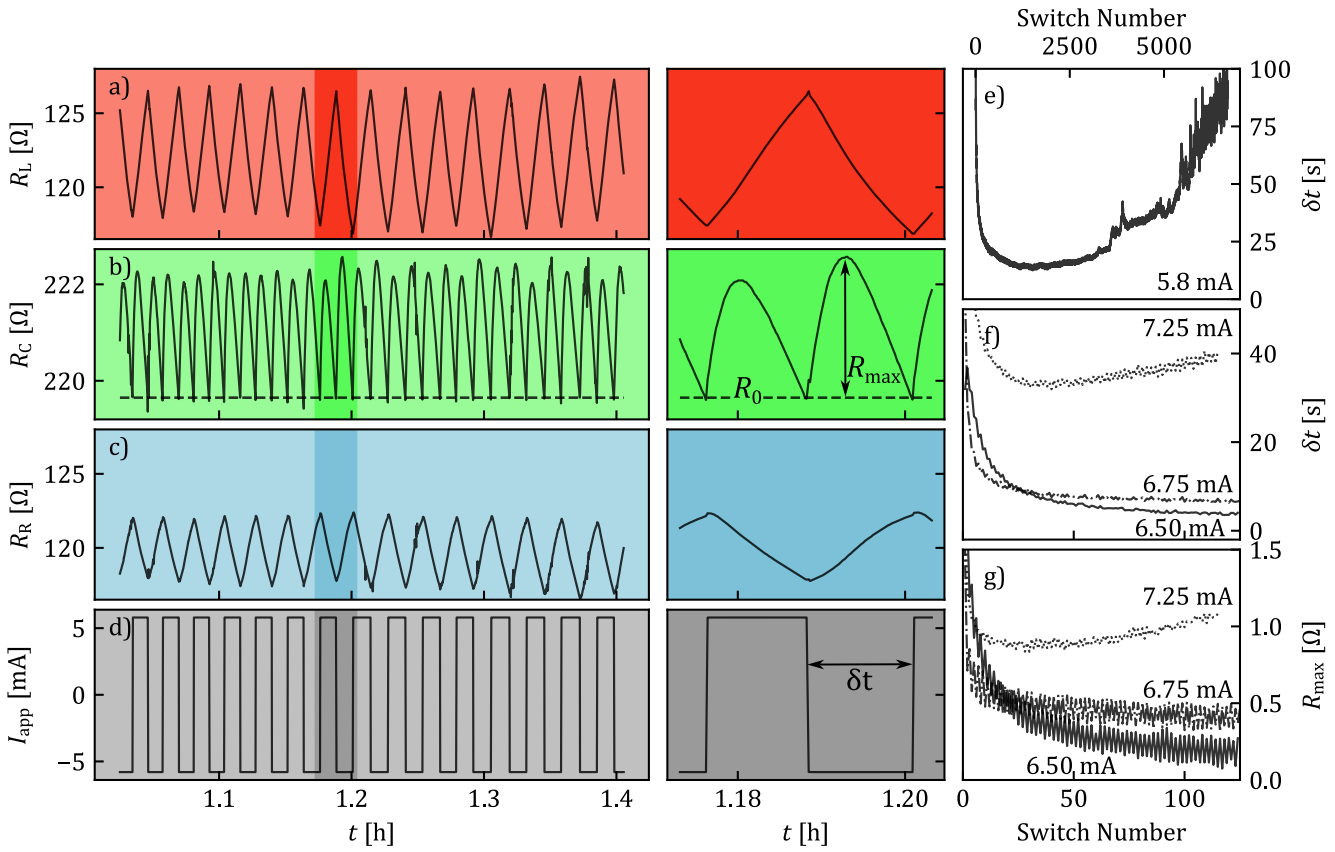

FIG. 2. Reversible resistive switching in a micropatterned YBCO film via square wave current of 5.8 mA amplitude and varying period. The red, green and blue panels correspond to the negative electrode (left), centre and positive electrode (right) resistance vs time measurements, while the grey panel shows the applied current. The switching resistance criterion (R_0) is set manually after a short initialization phase and is shown with the dashed horizontal line. This criterion is only checked in the middle constriction and determines the position at which the current polarity is switched. Note that the resistances of the left and right constrictions follow opposing trends, while the central constriction has a dome-shaped $R(t)$ curve. This is explained by an oxygen-vacancy counterflow following the current direction where the deoxygenation front repeatedly passes through the central constriction during switching. The insets are zooms on the highlighted sections of the data set. Experiments are performed in ambient conditions. (e) Evolution of the half-period δt (see definition in panel (d)) for a sample switching in a bipolar square wave current bias for $\sim$ 7000 switching cycles. Polarity is switched whenever R_C returns to a preset R_0, corresponding to a 1% increase of resistance from the pristine state. (f) Evolution of δt for three different current amplitudes performed on the same sample, the corresponding R_{max} evolution is shown in (g). These measurements were performed in the same device in chronological order, starting from the lowest current and increasing it progressively.

bers). This is consistent with the interpretation that higher drives induce more defects and thus lead to a premature failure of devices.[24]

Attempts to reproduce reversible resistance switching at low temperature ($T = 110$ K) show successful results, although the current needed to produce similar resistance change roughly doubles the one at room temperature. In all cases, the weak modifications induced in the normal state resistance by the switching process have no impact on the superconducting transition (see Appendix B), confirming that the maximum induced displacement of oxygen atoms in these experiments represents a minor perturbation, which in turn ensures reversibility.

B. Numerical results

Let us now apply finite element modelling (FEM) of electrically driven oxygen diffusion in order to gain a further understanding of the link between oxygen distribution and electro-transport measurements. To that end, we set up a simulation that mimicked the experimental protocol presented above and implemented it to reproduce the data of Fig. 2. As in the experiment, the two control parameters are the base resistance R_0, corresponding to the R_C value at which the polarity switch is triggered, and the applied current I_{app}.

The resulting resistance evolution for the three bridges obtained from the FEM is presented in Fig. 3. They

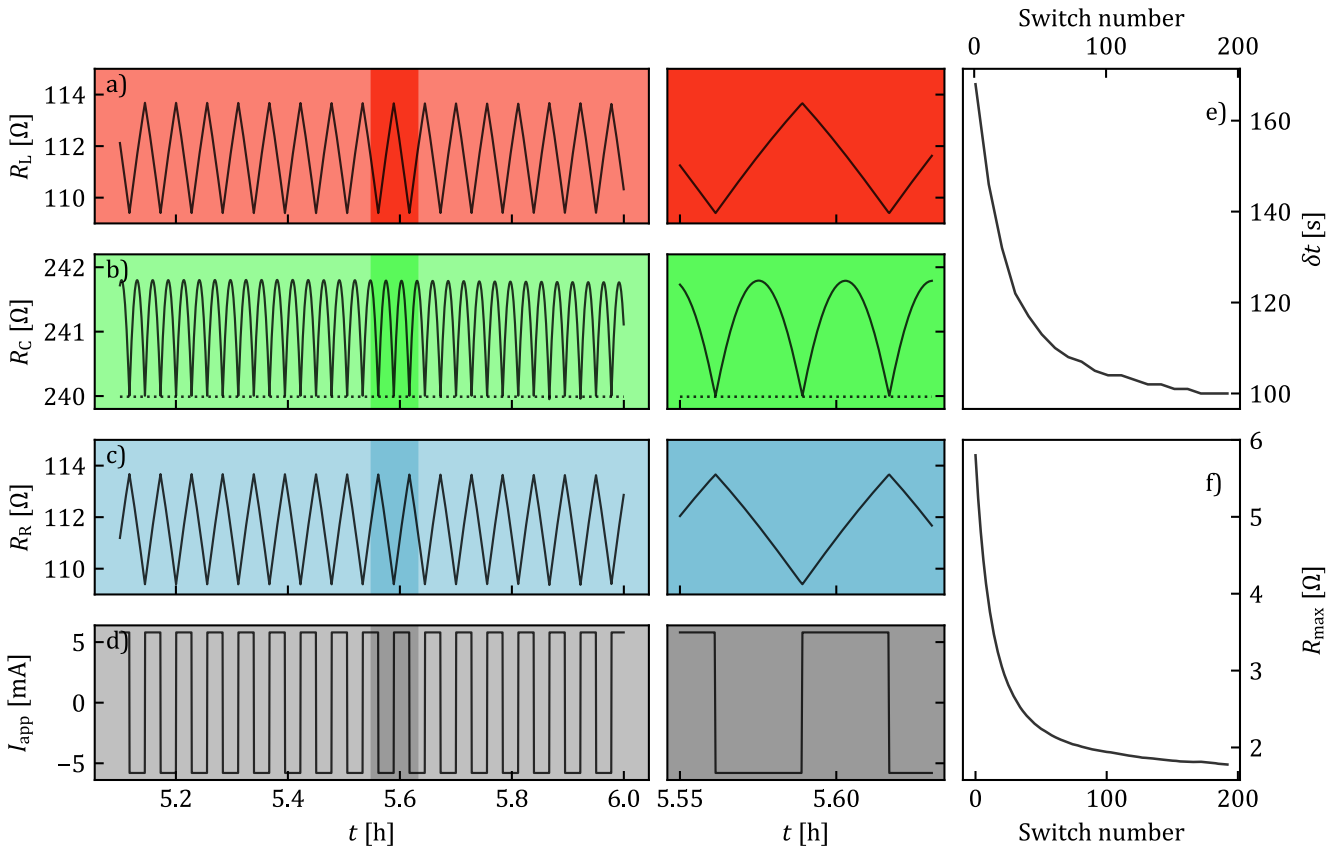

FIG. 3. Finite element modelling of the experimentally observed switching behaviour in YBCO thin film constrictions. The numerical model captures both the regular dome shape of R_C (b) and the opposite trends in R_L (a) and R_R (c), as well as the decreasing values of δt (e) and R_{max} (f).

clearly capture the most significant experimental features of the device shown in Fig. 2, hence supporting the interpretation of oxygen-V_O^{2+} counterflow as the main mechanism at the origin of resistive switching. Panels (e,f) also reproduce the settling of the value of R_{max} and δt to a constant value (R_{max}∼242 Ω and δt∼100 s), in accordance with the initial trend reported in Fig. 2(e-g).

Let us now dig further into the time evolution of the oxygenation and temperature during the switching process, as described by the numerical modelling. To that end, in Fig. 4a) we display a single $R_C(t)$ dome obtained for $I_{\rm app} = +5.8$ mA and $R_0 = 240$ Ω, after ∼1.5 h of periodic switching. A line profile of the oxygen content as described by the variable x is shown in panel (b) along the equatorial line of the model domain (see inset of panel b)) for 16 evenly spaced events between the i and vi markers. One should note the antisymmetric behavior of x across the $R(t)$ dome. The x-vs-position curves feature a single peak near the top of the dome (purple line and corresponding marker) and a double peak with corresponding double dip on the opposite side near the cusp of it. The secondary peaks/dips are best explained by geometrically induced current crowding near the voltage terminals, as shown in the color map representation of x, shown in c) for specific times labelled (i-vi) in a). The snapshot (i) in panel c) indicates the polarity during the highlighted dome. This polarity is inverted upon reaching the point (vi). Note that during the AC cycling, the doping level remains within a narrow region $0.89 < x < 0.91$, which is consistent with the superconducting transition being insensitive to the final resistance state during the switching process (see Appendix B). The panels in d) show dx (or similarly dx/dt), the local change of x between a given time-step and the previous one obtained 100 ms before. The temperature maps for the same instances (i-vi) is shown in e).

The initial distribution of oxygen concentration x shown in the snapshot (i) of panel c), reveals a large zone of rich oxygen content (blue) at the central constriction coexisting with a small (white) stripe of slight oxygen depletion, naturally explaining the low resistance value. Note that the right bridge exhibits depletion of oxygen (brown) whereas the left bridge is oxygenated but less than the central bridge. The polarity indicated in snapshot (i) pushes the V_O^{2+} to the left and the oxygen ions to the right. This causes the white stripe at the central constriction to move towards the left, whereas the blue zone will tend to displace towards the right side, as shown in

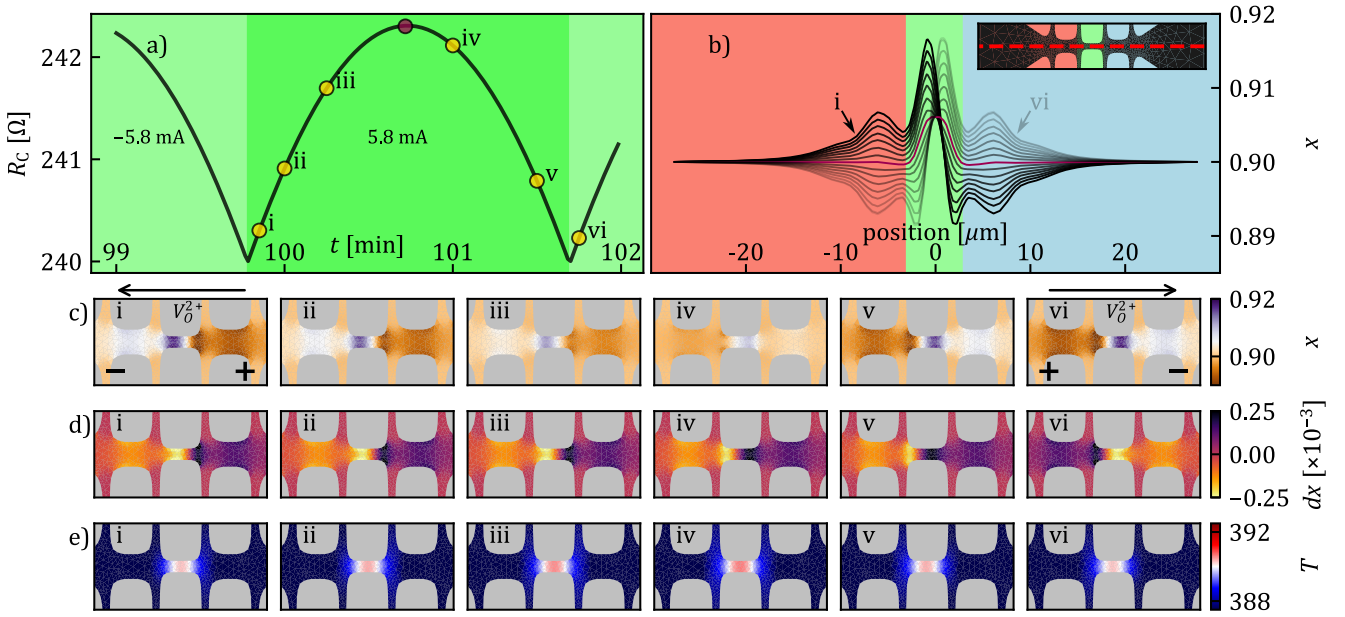

FIG. 4. a) Close up of the evolution of a single dome $R(t)$ from the finite element model. b) Values of the derived doping parameter x along the equatorial line of the model domain for 16 evenly spaced instances between the (i) and (vi) markers in a). The position at which the central (purple) curve is measured is indicated with the purple marker in a). c) Oxygen distribution maps (in x). d) Oxygen distribution differential maps (dx). e) Temperature profiles (T). Colormaps are taken from the model at the indicated points in a). The highlighted section corresponds to a positive current polarity pulse.

the snapshots (ii-iv) and panel b). At point (iv) the central bridge is more uniformly depleted in oxygen, which accounts for the high resistance value. At point (v), the situation is nearly mirror symmetric to that of picture (i). In other words, in the rising branch of the dome (i-iii) the center constriction is mostly a vacancy sink, then it becomes relatively equally distributed in (iv) and finally an oxygen sink in (v). These features become more compelling by plotting the differential of x, that is the change in oxygenation level from one simulation step to the next.

The dx maps show the rate of change of the oxygen concentration, with yellowish color when the rate is negative (oxygen content decreases) and darker color when the rate of change is positive (oxygen content increases). Since the polarity is kept constant for the considered dome, this rate of change remains roughly the same for (i-v). Note, however, that changes operate along the central bridge, averaging to negative rate of change for (i-iii) and positive for (iv,v). When the polarity of the current changes in the next dome (vi), the rate of change changes accordingly. Note that the dome is perfectly symmetric indicating that the initial current polarity does not introduce any asymmetry in the migration process. Detailed animations showing the time evolution of the oxygenation and temperature are presented in the Supplementary Material [25].

Figure 4 also reveals the presence of wave-like deoxygenation fronts in the x and dx images, similar to those previously reported in Ref. [17]. The wave nucleates at points of large current crowding,[26] that is, at the junctions of the constrictions and at the voltage lines, resulting in the double peak shape of the plot in Figure 4b). It is interesting to point out that vacancy migration can form a shock wave with a well-defined front without the need to invoke current crowding, as described in Ref.[27]. The bottom row shows that the temperature profile of the sample remains roughly homogeneous, with peak temperatures of ∼90 K above room temperature, replicating the experimental observation elaborated upon in Appendix A. As expected, close to the peak of the dome at point (iv), a higher resistance implies more Joule heating and consequently higher temperature.

Although the proposed model satisfactorily accounts for the experimentally observed behaviour of the sample, the simulations do not seem to replicate all details, such as the alternating $R_{\max}$ values. In order to explain the origin of the varying dome height for positive and negative bias, as shown in Fig. 2(b), we ran FEM simulations on an intentionally asymmetric device and compared it to a symmetric one, as depicted in Fig. 5. In the asymmetric structure (lower panel), the right constriction is 1 μm wider than the left one. Under this circumstance, the right constriction starts in a lower resistance state and never reaches the same peak oxygenation state as the left one, which is well illustrated in Appendix B. During positive polarity, oxygen flows left to right, but the flow is limited due to reduced current density and lower tem-

perature in the wider (right) constriction. On reversal, the wider constriction, which is colder and is comparably deoxygenated, traps vacancies and, in this way, extends the oxygen flow in the left constriction, leading to a larger reduction of R_C during negative pulses. Thus, the experimentally observed alternating R_{max} values could be explained by invoking geometrical asymmetries or likely other sources of asymmetries in the microstructure.

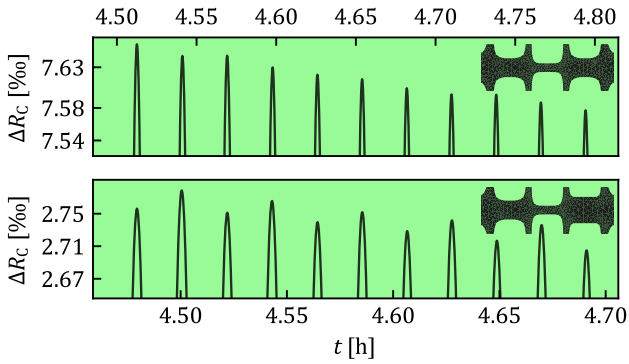

FIG. 5. Section of a finite element modelling simulation on a symmetric (upper panel) and an asymmetric (lower panel) mesh where the right constriction is 1 μm wider than the left one (see inset). The asymmetry induces an alternating trend in the evolution of R_C where positive polarity periods show higher $R_{\max}$. The low observed amplitude results from the relatively long time needed for the system to settle.

IV. CONCLUSION

We investigated the reversible (low on-off amplitude) resistive switching by selective electromigration of oxygen in YBCO through a simple electrical protocol. The methodology can be easily replicated and applied to a broad family of oxide materials.[12, 28] We study the resilience of these devices to cyclic stress and the evolution of the resistance of multiple constrictions in series. The observed oxygen-vacancy counterflow is validated via finite element modelling. The presented results provide insights into the nature of the wavelike movement of the deoxygenation front and local temperature under low-frequency AC current stress.

The presented research supports the interpretation of electrical oxygen-V_O^{2+} redistribution as the driving mechanism for switching. It has been demonstrated that electric field-induced transition to high resistance states occurs through the generation of $YBa_2Cu_4O_7$ (Y124) intergrowths with a large number of oxygen vacancies.[29] Although we expect that a similar mechanism applies when electromigration leads to large on-off amplitudes [16], it remains unclear in the present case if clusters of Y124 phase develop or a more uniform redistribution of oxygens takes place. Judging by the insensitivity of superconducting transitions to the actual normal state resistance, we believe that disconnected clusters or filaments of depleted oxygen concentration coexist with optimally doped regions. FEM simulations were able to qualitatively, and to a certain extent, quantitatively reproduce the experimental findings. In the present report, the period of the dome $\delta t \sim 20$ s and the propagation distance of the deoxygenated front ~ 5 μm points to a very slow diffusion process. The maximum switching speed remains to be explored either by electric gating or electromigration. The phenomena of electromigration at ns time scale are expected to generate little Joule heating, thus requiring substantially higher current pulses to achieve resistance changes similar to the one explored in this work. As a last remark, it is instructive to point out that the trade-off between large amplitude switching and reversibility suggests that electromigration in YBCO may, at the µm scale investigated here, not represent a competitive alternative to memristive effect based on electric-field gating.[14] The latter permits much larger amplitude variations than the ones here reported and yet within a reversible regime and requiring less power consumption.[10] Current-driven switching still offers advantages in ease of implementation through simpler fabrication and a lower number of terminals, as well as the possibility to more comfortably access a higher number of resistive states in the devices, which still may make them appealing for neuromorphic applications.

V. ACKNOWLEDGEMENT

The authors acknowledge support from Fonds de la Recherche Scientifique - FRS-FNRS (Research Fellowship ASP), COST action SUPERQUMAP (CA 21144), Spanish Ministry of Science and Innovation MCIN/AEI/10.13039/501100011033/ through the "Severo Ochoa" Programme for Centres of Excellence MaTrans42 CEX2023-001263-SCEX2019-000917-S, HT-SUPERFUN PID2021-124680OB-I00 funded by ERDF A way of making Europe. The Spanish Nanolito networking project (RED2022-134096-T) and Catalan Government (2021-SGR-00440). S.M. acknowledges support from FRS-FNRS Research Fellowship ASP under the grant 1.A.320.21F. S.M and D.S contributed equally to this work.

Appendix A: Initial Thermalization Phase

The micrometric constrictions investigated in this work are exposed to high current densities during extended periods of time and, therefore, undergo substantial Joule heating. In the initial phase, the sample takes some time before stabilizing at the final temperature. The data presented in the body of the manuscript corresponds to the measurements acquired at thermal equilibrium (i.e. under isothermal conditions), whereas the initial thermalization phase is removed. In order to estimate the charac-

teristic time-scale necessary to achieve the thermal equilibrium, we wired a second device 3.5 mm away from the sample under high bias (7.5 mA) and used this second device as a thermometer, i.e. its resistance is monitored with a low DC current (10 μA). The sketch in Fig. 6(d) shows the sample-thermometer in grey colour and the high-biased device with RGB colour code associated with each of the three bridges in series. The corresponding resistance evolution as a function of time is displayed using the same colour code in panels (a-c). These experiments suggest that for the utilized 5×5 mm^2 LAO substrates, the thermalization occurs on the order of minutes after turning on the high-current bias.

The resistance of the bridges (Fig. 6(a-c)) and that of the thermometer (Fig. 6(e)) asymptotically approach their final values R_f roughly following an exponential dependence as demonstrated by the semi-log plots shown in the insets of these panels. A fit to this data using the equation,

$$R(t) = R(0) + (R_f - R_0)(1 - e^{-t/\tau}), \qquad \text{(A1)}$$

allow us to extract a relaxation time $\tau \approx 2$ min. In addition, by extracting the temperature coefficient of resistance α from fits to $R(T) = R_0(1-\alpha(T-T_0))$, we can estimate the temperature of the sample once the thermal equilibrium is reached ($T \approx 390$ K) and the temperature of the substrate 3.5 mm away from that hot spot, which rises to about 11 K above the room temperature. The fact that the temperature of the constriction during the switching process remains relatively low, is consistent with the observation of no loss of oxygen out of the sample. An additional manifestation of the thermalization process has been obtained directly from the thermometer attached to the bulky cold finger of the cryostat as schematically shown in the inset of Fig. 6(g). Panel (f) of this figure shows the evolution of the resistance of the central constriction at 110 K and panel (g) shows the evolution of the temperature simultaneously picked up by the thermometer in the cold finger.

The 90 K increase in temperature during the resistive switching plays an important role in the the electromigration of oxygen vacancies which is a thermally activated process and therefore, grows exponentially with temperature. More specifically, increasing the temperature permits to trigger the electromigration process at relatively low currents. For instance, at room temperature a current of about 6 mA is needed to induce oxygen migration whereas at 110 K the onset of electromigration happens for currents values about 13 mA.

Appendix B: Invariability of the Superconducting Transition after Cycled Electromigration

Figure 7 shows the resistance versus temperature $R(T)$ response, measured with a dc current of 10 µA after performing repeated cycling switching processes at 110 K using a switching current of 13 mA. The color code of the panels is as described in Fig. 1 and corresponds to the three bridges in series. The figure shows that the superconducting transition remains unaffected by the weak switching process. Indeed, the onset of superconductivity is the same irrespective of whether the switching process is halted at the the end of the positive or negative current polarity pulse, or after 5 h cycled switching, and remains close to the response of the virgin sample.

[1] R. Ramesh and D. G. Schlom, Creating emergent phenomena in oxide superlattices, Nat. Rev. Mater. **4**, 257 (2019).

[2] E. Janod, J. Tranchant, B. Corraze, M. Querré, P. Stoliar, M. Rozenberg, T. Cren, D. Roditchev, V. T. Phuoc, M. Besland, and L. Cario, Resistive switching in mott insulators and correlated systems, Adv. Funct. Mater. **25**, 6287 (2015).

[3] R. A. De Souza, Oxygen diffusion in $SrTiO_3$ and related perovskite oxides, Adv. Funct. Mater. **25**, 6326 (2015).

[4] J. D. Jorgensen, B. W. Veal, A. P. Paulikas, L. J. Nowicki, G. W. Crabtree, H. Claus, and W. K. Kwok, Structural properties of oxygen-deficient $YBa_2Cu_3O_{7-\delta}$, Phys. Rev. B **41**, 1863 (1990).

[5] L. Bégon-Lours, V. Rouco, A. Sander, J. Trastoy, R. Bernard, E. Jacquet, K. Bouzehouane, S. Fusil, V. Garcia, A. Barthélémy, M. Bibes, J. Santamaría, and J. E. Villegas, High-temperature-superconducting weak link defined by the ferroelectric field effect, Phys. Rev. Appl. **7**, 064015 (2017).

[6] A. M. Perez-Muñoz, P. Schio, R. Poloni, A. Fernandez-Martinez, A. Rivera-Calzada, J. C. Cezar, E. Salas-Colera, G. R. Castro, J. Kinney, C. Leon, J. Santamaria, J. Garcia-Barriocanal, and A. M. Goldman, In operando evidence of deoxygenation in ionic liquid gating of $YBa_2Cu_3O_{7-x}$, Proc. Natl. Acad. Sci. U. S. A. **114**, 215 (2017).

[7] A. S. Dhoot, S. C. Wimbush, T. Benseman, J. L. MacManus-Driscoll, J. R. Cooper, and R. H. Friend, Increased T_c in electrolyte-gated cuprates, Adv. Mater. **22**, 2529 (2010).

[8] A. Schulman and C. Acha, Cyclic electric field stress on bipolar resistive switching devices, J. Appl. Phys. **114**, 243706 (2013).

[9] A. Palau, A. Fernandez-Rodriguez, J. C. Gonzalez-Rosillo, X. Granados, M. Coll, B. Bozzo, R. Ortega-Hernandez, J. Suñé, N. Mestres, X. Obradors, and T. Puig, Electrochemical tuning of metal insulator transition and nonvolatile resistive switching in superconducting films, ACS Appl. Mater. Interfaces **10**, 30522 (2018).

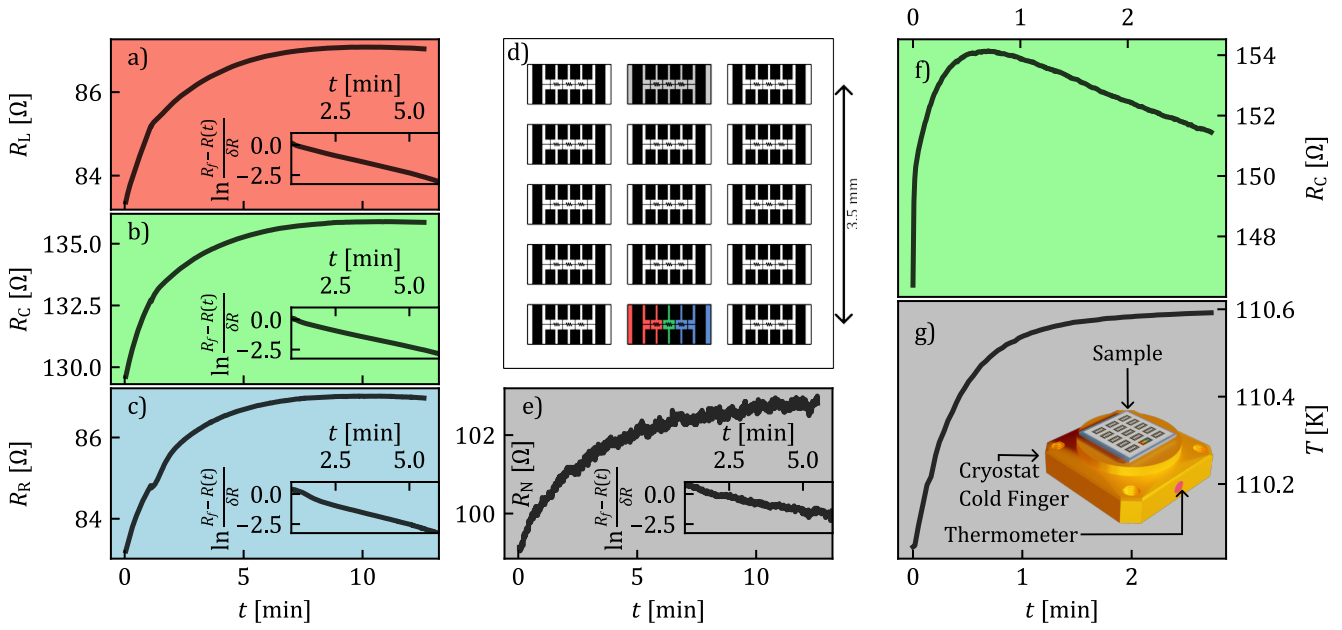

FIG. 6. Demonstration of the heating power effected by a device under experiment conditions. The three plots in the left column (red-green-blue) a)-c) show the measured 4-point resistance of a triple constriction device conducting 7.5 mA of DC current, with the panels representing the left, centre and right constrictions, respectively. The measured resistances increased in all three bridges before settling to stable values at around 6 min after starting, implying that Joule-heating caused the thermalization of the chip. To confirm this heating effect, another device on the opposite side of the chip is wired, and its central constrictions' 4-point resistance is recorded with a low DC current (10 μA) simultaneously with the high-current measurement in the device under test. The resulting measurement is shown in panel e) with a grey background. The two devices are positioned as shown in the illustration in panel d), the devices being colored as in the other panels. The central constrictions of the devices are ∼3.5 mm apart. The identical shape of the resistance curves serves well to illustrate that the heating of the high-current device is enough to affect the whole chip. Measurement of the heating of the cryostat cold finger due to Joule heating in a YBCO microconstriction passing 7.5 mA DC current at 110 K are shown in panels f) and g). f) shows the resistance evolution of the central constriction R_C with the characteristic dome shape discussed in the main text, while panel g) shows the temperature read at the cryostat cold finger with a copper thermometer. Note the temperature increase of ∼500 mK due to the heat generated in the sample. The inset in the grey panel shows a rendition of the mounted sample on the gold base of the cold finger, illustrating the distance from a working device to the thermometer.

[10] A. Lagarrigue, *Electrical and spin switching effects in high-temperature superconducting devices*, Ph.D. thesis, Université Paris-Saclay (2023).

[11] E. Trabaldo, A. Kalaboukhov, R. Arpaia, E. Wahlberg, F. Lombardi, and T. Bauch, Mapping the phase diagram of a $YBa_2Cu_3O_{7-\delta}$ nanowire through electromigration, Phys. Rev. Appl. **17**, 024021 (2022).

[12] S. Marinković, A. Fernández-Rodríguez, E. Fourneau, M. Cabero, H. Wang, N. D. Nguyen, J. Gazquez, N. Mestres, A. Palau, and A. V. Silhanek, From electric doping control to thermal defect nucleation in perovskites, Adv. Mater. Interfaces **9**, 2200953 (2022).

[13] J. J. Yang, D. B. Strukov, and D. R. Stewart, Memristive devices for computing, Nat. Nanotechnol. **8**, 13 (2013).

[14] C. Acha and M. J. Rozenberg, Non-volatile resistive switching in the dielectric superconductor $YBa_2Cu_3O_{7-\delta}$, J. Phys.: Condens. Matter **21**, 045702 (2009).

[15] M. J. Rozenberg, M. J. Sánchez, R. Weht, C. Acha, F. Gomez-Marlasca, and P. Levy, Mechanism for bipolar resistive switching in transition-metal oxides, Phys. Rev. B **81**, 115101 (2010).

[16] S. Marinković, A. Fernández-Rodríguez, S. Collienne, S. B. Alvarez, S. Melinte, B. Maiorov, G. Rius, X. Granados, N. Mestres, A. Palau, and A. V. Silhanek, Direct visualization of current-stimulated oxygen migration in $YBa_2Cu_3O_{7-\delta}$ thin films, ACS Nano **14**, 11765 (2020).

[17] S. Collienne, S. Marinković, A. Fernández-Rodríguez, N. Mestres, A. Palau, and A. V. Silhanek, Electrically-driven oxygen vacancy aggregation and displacement in $YBa_2Cu_3O_{7-\delta}$ films, Adv. Electron. Mater , 2101290 (2022).

[18] S. J. Rothman, J. L. Routbort, and J. E. Baker, Tracer diffusion of oxygen in $YBa_2Cu_3O_{7-\delta}$, Phys. Rev. B **40**, 8852 (1989).

[19] R. Hoffmann-Vogel, Electromigration and the structure of metallic nanocontacts, Appl. Phys. Rev. **4**, 031302 (2017).

[20] COMSOL, Understanding the fully coupled vs. segregated approach and direct vs iterative linear solvers, available online: www.comsol.com/support/knowledgebase/1258. (Accessed: 2024-04-01).

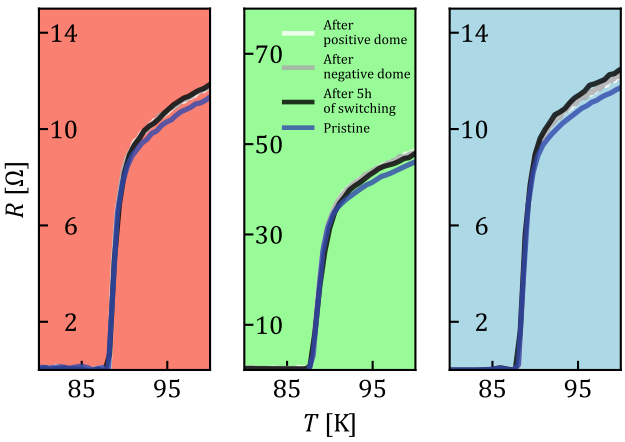

FIG. 7. Resistance as a function of temperature for the three bridges en series. The background color corresponds to that introduced in Fig. 1. $R(T)$ were obtained with a dc current of 10 µA after different switching states: virgin sample (green), at the end of a positive current pulse (blue), at the end of a negative current pulse (magenta), and after 5 h of cycled switching process.

[21] K. Semba and A. Matsuda, Superconductor-to-insulator transition and transport properties of underdoped $YBa_2Cu_3O_{7-y}$ crystals, Phys. Rev. Lett. **86**, 496 (2001).

[22] S. Marinković, E. Trabaldo, S. Collienne, F. Lombardi, T. Bauch, and A. V. Silhanek, Oxygen ordering in untwinned $YBa_2Cu_3O_{7-\delta}$ films driven by electrothermal stress, Phys. Rev. B **107**, 014208 (2023).

[23] Y. V. Pershin and M. Di Ventra, Memory effects in complex materials and nanoscale systems, Adv. Phys. **60**, 145 (2011).

[24] A. Schulman and C. Acha, Cyclic electric field stress on bipolar resistive switching devices, J. Appl. Phys. **114**, 243706 (2013).

[25] See Supplemental Material at [URL will be inserted by publisher] for two animations of the simulated time-dependent parameter change during the process of AC electromigration.

[26] F. B. Hagedorn and P. M. Hall, Right-Angle Bends in Thin Strip Conductors, J. Appl. Phys. **34**, 128 (1963).

[27] S. Tang, F. Tesler, F. G. Marlasca, P. Levy, V. Dobrosavljević, and M. Rozenberg, Shock waves and commutation speed of memristors, Phys. Rev. X **6**, 011028 (2016).

[28] I. L. Goulatis, R. V. Vovk, and A. I. Chroneos, Oxygen diffusion in $RBa_2Cu_3O_{7-\delta}$ superconductors: A brief review, Low Temp. Phys. **49**, 1271 (2023).

[29] J. Alcalà, A. Fernández-Rodríguez, T. Günkel, A. Barrera, M. Cabero, J. Gazquez, L. Balcells, N. Mestres, and A. Palau, Tuning the superconducting performance of $YBa_2Cu_3O_{7-\delta}$ films through field-induced oxygen doping, Sci. Rep. **14**, 1939 (2024).